Size-efficient metamaterial absorber at low frequencies: Design, fabrication, and characterization

Bui Xuan Khuyen,[1] Bui Son Tung,[1] Nguyen Van Dung,[1] Young Joon Yoo,[1] Young Ju Kim,[1] Ki Won Kim,[2] Vu Dinh Lam,[3] Jun Gyu Yang,[4] and YoungPak Lee[1,a)]
[1]*Department of Physics, Quantum Photonic Science Research Center and RINS, Hanyang University, Seoul 133-791, South Korea*
[2]*Department of Information Display, Sunmoon University, Asan, South Korea*
[3]*Institute of Materials Science, Vietnamese Academy of Science and Technology, 18 Hoang Quoc Viet, Hanoi, Vietnam*
[4]*National Radio Research Agency, Naju, South Korea*

(Received 21 March 2015; accepted 16 June 2015; published online 26 June 2015)

We numerically and experimentally demonstrated a metamaterial perfect absorber (MPA) in MHz region based on a planar sandwiched metal-dielectric-metal structure. First, the single-peak perfect absorption was obtained at 400 MHz. The ratios of the periodicity of unit cells and the thickness to the absorption wavelength are 1/12 and 1/94, respectively. The advantage of structural design and the mechanism for the low-frequency MPA are described in detail by the comparison between calculation, simulation, and experiment. Influence of the incident angle of electromagnetic (EM) wave for both transverse-electric (TE) and transverse-magnetic (TM) polarization on absorption was also investigated, and the absorption was maintained to be above 95% at incident angles up to 30°. Finally, we propose a self-asymmetric structure, which induces the dual-band perfect absorption in the same range of frequency. The EM behavior of the excitation modes and the mechanism of the dual-band MPA are clearly explained. Especially, when two resonance modes are finely controlled to be close enough, the bandwidth (full width at half maximum) of MPA is enhanced to be nearly wider twice than that in case of single-peak perfect absorption. The enhanced bandwidth is still well preserved by varying the incident angle up to 30° for both TE and TM polarization. The results were also confirmed by both simulation and experiment. Our work is promising for potential practical applications in the radio range, such as radio-frequency shielding devices, single/dual-frequency filters, and switching devices. © *2015 AIP Publishing LLC*.
[http://dx.doi.org/10.1063/1.4923053]

I. INTRODUCTION

Since more than a decade ago, metamaterials (MMs) have attracted many researchers in the whole world because of exotic properties, which cannot be found in natural materials. MMs are known as artificial materials including both electric and magnetic components, which play role as artificial "atoms" or "molecules." These artificial elements are flexible and easily manipulated to provide many precious effects, such as negative refractive index,[1,2] slow light,[3–5] super resolutions,[6,7] and invisibility cloaking.[8,9] So far, many works relevant to MMs have been investigated in wide frequency range from radio,[10] microwave,[11] THz,[12] infrared[13] to visible.[14] Recently, another fascinating application, the so-called metamaterial perfect absorber (MPA), was discovered by Landy *et al*. in 2008.[15] Thenceforth, MPAs have been effervescently studied in the new materials science field and promising for wide application areas, such as thermal images,[16,17] solar cell,[18] sensor,[19] and photodetector.[20] The absorption mechanism of MPA can be understood based on the effective medium theory.[21] By controlling the real and the imaginary parts of electric permittivity $\varepsilon(\omega)$ and magnetic permeability $\mu(\omega)$, the effective impedance of MPA, $Z = \sqrt{\mu(\omega)/\varepsilon(\omega)}$, is perfectly matched with free space, and the imaginary part of refractive index is extremely enhanced. Consequently, both reflection and transmission of EM radiation from MPA are eliminated.[15,22] In this way, the EM energy is perfectly absorbed inside the MPA.

Most of MPAs have been presented in GHz[15,23–25] and THz[26–28] ranges, since the first demonstration by Landy. Nowadays, the development of telecommunication devices based on MPA is one of the promising highlighted fields. The advantages of MPA are being extended for wide applications such as the improved readability within RFID (radio-frequency identification) portals,[29] power imaging purposes,[30] chipless radio-frequency identification tags,[31] and sub-GHz wireless systems.[32] However, for real applications in the radio region, the scale-down of reported MPA structures is a big challenge due to the limitation of allowed dimensions for the unit cell. For instance, in Ref. 32, the MPA has periodic unit-cell dimension of $\sim\lambda/2$ and a thickness of $\sim\lambda/44$ at 686 MHz, where λ is the operation wavelength. In many situations, these sizes are still too large to be applied in practical devices operating at lower frequencies. In our work, therefore, we introduce a small and thin MPA working in the MHz region using only traditional low-cost materials, FR-4 dielectric and copper. By a proper design, the single-peak perfect absorption at low frequency was

a)Email: yplee@hanyang.ac.kr

induced by the fundamental magnetic resonance. In order to exploit the advantage of the proposed MPA, moreover, we propose a self-asymmetric structure, which produces the dual-band perfect absorption. By following this way, the full width at half maximum (FWHM) of absorption spectrum can be easily enhanced by partially overlapping of two resonance modes. For both single-peak and enhanced-bandwidth MPAs, the dependence of absorption on the incident angle of EM wave was investigated in detail. Our work would provide high benefits for the practical applications in the radio region.

II. SIMULATION AND EXPERIMENT SETUP

The proposed MPA is a periodic arrangement of the unit cell depicted in Fig. 1(a). A patterned metallic front layer is composed of four quarters of disk localized at corners, which are linked together by slender wires. The front layer is separated from a continuous back metallic layer by a dielectric spacer. The lattice constant of unit cell is $a = 62.5$ mm in the x-y plane. The front and the back metallic layers have a thickness of $t_m = 0.035$ mm. The radius of the quarter of disk and the width of wire are selected to be $r = 28.5$ mm and $w = 0.3$ mm, respectively. The substrate is FR-4 with a dielectric constant of 4.3 and a dielectric loss tangent of 0.025. The metal is chosen as copper with an electric conductivity of $\sigma = 5.8 \times 10^7$ S/m. Figures 1(b) and 1(c) show the real samples of single-peak and dual-band MPAs, respectively, which were fabricated by the conventional printed-circuit-board process with size of 60×60 cm^2. In case of the single-peak MPA, the thickness of FR-4 layer is $t = 8.0$ mm and the gaps are $g_1 = g_2 = 0.15$ mm. In the case of the asymmetric MPA, the FR-4 thickness is chosen as $t = 14.0$ mm, while the gaps g_1 and g_2 are 0.15 and 0.6 mm, respectively.

Figure 1(d) presents the experimental configuration of measurement. A Hewlett-Packard E8362B network analyzer is connected to two horn linearly polarized standard-gain antennas (685×530 mm^2), which are used for illuminating the microwave beam on the sample and receiving the reflected beam from the sample with an incident angle of 10°. The sample is held by a bracket and placed at a proper distance of 2.0 m from middle point of two horn antennas to center of the MPA sample. Our simulated results are performed by a commercial program, CST Microwave Studio software.[33] In simulations, the polarization of incident EM wave was set as shown in Fig. 1(a). Generally, when EM wave is propagated through MPA, the absorption can be calculated as $A(\omega) = 1 - |S_{11}(\omega)|^2 - |S_{21}(\omega)|^2$, where $S_{11}(\omega)$ and $S_{21}(\omega)$ are the reflection and the transmission parameters, respectively. Because the back layer is a continuous metallic plane, the incident EM wave is prevented from transmitting. Therefore, the transmission is zero and the absorption is expressed as $A(\omega) = 1 - |S_{11}(\omega)|^2$.

III. RESULTS AND DISCUSSION

First, the absorption spectrum of single-peak MPA is demonstrated in Fig. 2(a). The simulated and the experimental results are quite coincident. There is a nearly perfect absorption peak at around 400 MHz in both simulation and measurement. The absorption is 98.6% (FWHM of 4.0%) and 99.7% (FWHM of 6.3%) at 400 MHz in simulation and measurement, respectively. The small discrepancy in spectrum shape between simulated and experimental results might be due to the imperfection of the fabrication. It is noteworthy that the periodicity and the thickness of MPA are very small with respect to the operation wavelength: $a = \lambda/12$ and $t = \lambda/94$, where λ is the resonant wavelength (in mm). These values are smaller than those reported in previous works.[29,32]

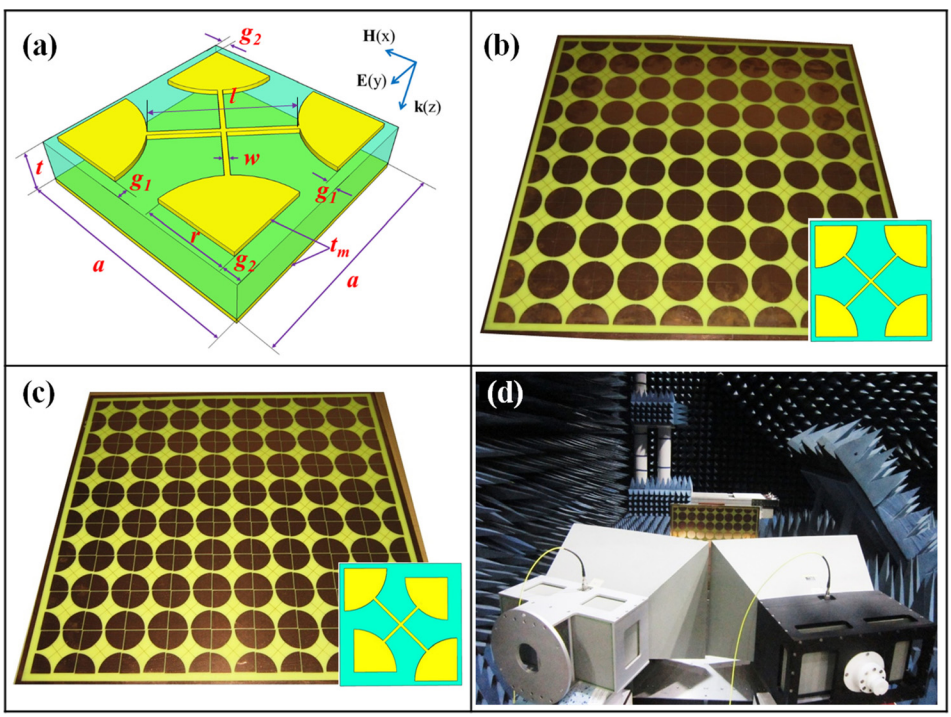

FIG. 1. (a) Unit cell of proposed MPA. Photos of fabricated (b) single-peak and (c) dual-band sample. Insets in (b) and (c) are the unit cells, corresponding to single-peak and dual-band MPA structures, respectively. (d) Experimental set-up for the measurement.

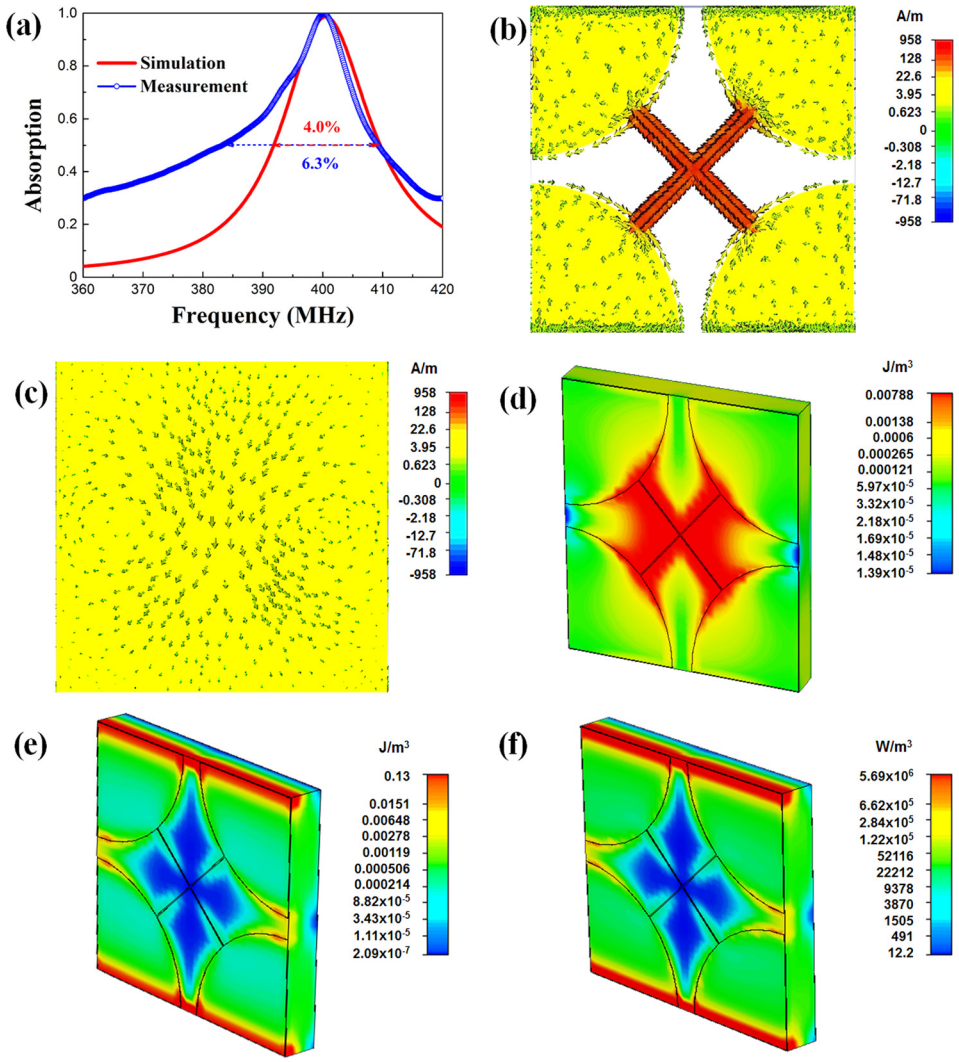

FIG. 2. (a) Simulated and measured absorption spectra of single-peak MPA. Red and blue dashed arrows display the FWHM values corresponding to the simulated and the experimental absorption spectrum, respectively. Induced surface currents on (b) front and (c) back layers at 400 MHz. 3-dimensional distributions of (d) magnetic energy, (e) electric energy, and (f) power loss at the resonant frequency.

In order to understand more clearly about the nature of perfect absorption, the simulated surface-current and magnetic-energy distributions at 400 MHz are presented. As shown in Figs. 2(b) and 2(c), owing to the polarization of EM field, the induced surface currents flow in bottom-up direction on the front layer. The induced charges are confined to the edges of the quarters of disk, and the corresponding mirror image of opposite charges is formed in the ground metallic plane. This result indicates that the anti-parallel surface currents, which are an evidence for a magnetic resonance, are induced on the top and the bottom metallic layers. Simultaneously, the top metallic patch plays an important role in the coupling between MPA and external EM field to satisfy the impedance matching condition. Accordingly, the total energy of incident EM wave is consumed inside MPA, as indicated in Fig. 2(a). Due to the special design of our MPA, the induced currents have high magnitude when passing through the slender wires. The phenomenon makes the magnetic energy distributed as shown in Fig. 2(d). At the position corresponding to slender wires, the magnitude of magnetic energy is strongly enhanced. In addition, the magnetic resonance also causes the distributions of induced electric energy and power loss as shown in Figs. 2(e) and 2(f), respectively. Evidently, the loss of incident EM wave is appreciably dissipated inside the dielectric space in the area between adjacent unit cells, where the induced electric field is large owing to the formed effective capacitors [Fig. 2(f)]. In other words, by exploiting the magnetic resonance, the dielectric loss plays dominant role in the energy dissipation of this MPA.[15,23,24,34]

To evaluate the preeminent advantage of the proposed MPA, we investigated the contributions of structural components to the operation frequency range theoretically and by simulation. As aforementioned for Fig. 2, the underlying physics of MPA is the magnetic resonant phenomenon. Therefore, the absorption frequency can be quantitatively defined by the equivalent inductor-capacitor (LC) circuit model, which has been reported elsewhere.[35,36] The equivalent circuit of our MPA is presented in Fig. 3(a) (the resistor element is ignored for simplicity in this case). The effective inductance (L_m) of front and back metallic layers can be approximately expressed by[37]

$$L_m = \frac{\mu_o \pi (t + 2t_m)}{2} + \frac{\mu_o l}{2\pi}\left[\ln\frac{2l}{w} + 0.5 + \frac{w}{3l} - \frac{w^2}{24l^2}\right]. \quad (1)$$

The interaction between copper-patterned layer and bottom continuous copper plane can be represented by the effective capacitance (C_m), which is given by Eq. (2). The air capacitance (C_e) between adjacent unit cells along E direction can be estimated by Eq. (3)[35]

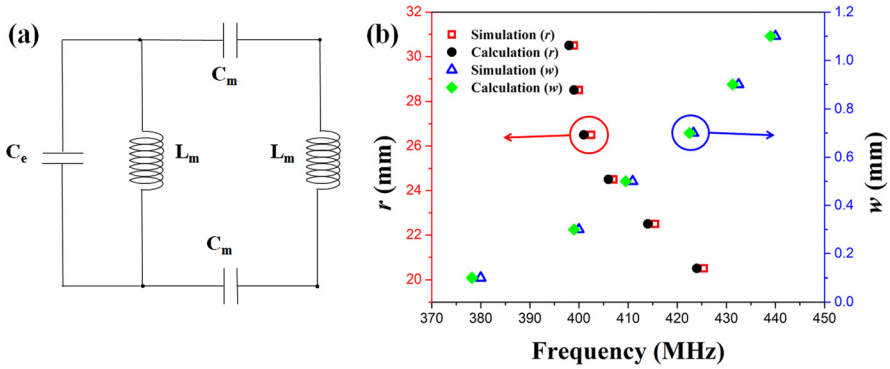

FIG. 3. (a) Equivalent circuit of the discussed MPA. (b) Simulated and calculated absorption frequencies according to radius of the quarter of disk (r) and width of slender wire (w). Red-square and blue-triangle symbols represent the simulated results, while the calculated results are denoted in black dots and green diamonds.

$$C_m = \frac{\varepsilon\varepsilon_o c_1}{t}[\pi r^2 + 2wl], \tag{2}$$

and

$$C_e = \frac{\pi\varepsilon_o r}{\ln(g_1/t_m)}. \tag{3}$$

For the equations above, μ_0 and ε_0 are the free-space permeability and permittivity, respectively. ε is the permittivity of FR-4, and c_1 is a geometrical factor varying from 0.2 to 0.3. The total impedance of oscillator circuit is given by

$$Z = \frac{i\omega L_m}{1-\omega^2 L_m C_e} + \frac{2}{i\omega C_e} + i\omega L_m. \tag{4}$$

Consequently, the magnetic resonant frequency can be derived by the condition of $\mathrm{Im}(Z) = 0$ to be

$$f_m = \frac{\omega_m}{2\pi} = \frac{1}{2\pi}\sqrt{\frac{C_m + C_e - \left(C_m^2 + C_e^2\right)^{1/2}}{L_m C_m C_e}}. \tag{5}$$

Since the influence of C_e ($\approx 0.1C_m$) in the equivalent circuit is not significant, we can approximately determine the magnetic resonance frequency as $f_m = 1/2\pi\sqrt{L_m C_m}$, which is inversely proportional to the square root of inductance and capacitance. For operation of MPA at low frequency, the key idea of our suggestion is combination of slender wires (size of $l \times w$) and four quarters of disk (radius r) in order to achieve large inductance and capacitance simultaneously. The dependences of calculated and simulated absorption frequencies on geometrical components r and w are shown in Fig. 3. It is clearly seen that the calculated and simulated results are in good agreement. When r is increased from 20.5 to 30.5 mm, while w is kept to be 0.3 mm, the absorption peak is red-shifted from 425 to 399 MHz. In contrast, in case of varying w from 0.1 to 1.1 mm, while the radius r is fixed to be 28.5 mm, the absorption peak is significantly blue-shifted from 380 to 440 MHz. These results explain why our proposed design of MPA, the large-radius quarter of disk and small-width wire leading to maximizing C_m and L_m, is appropriate for low frequency absorption.

Next step, we investigated the dependence of absorption on a wide range of incident angle for both transverse-electric (TE) and transverse-magnetic (TM) polarization. Figure 4(a) shows the evolution of simulated absorption spectrum when the angle of incidence θ is increased from 0 to 40° for TE polarization. Evidently, the simulated absorption reaches 98.6% for 400 MHz at $\theta = 0$ and gradually reduced to be 93% at $\theta = 40°$. In order to verify the simulation results, the corresponding experiment was carried out as shown in Fig. 4(b). The evolution of measured absorption spectrum agrees well with the simulation. The measured absorption decreases from 99.7% to 88% when θ increases from 10° to 40°. In addition, the absorption frequency is nearly unchanged according to θ. The slight reduction of absorption according to incident angle can be explained by the coupling between external magnetic field of the incident EM wave and MPA. When θ is larger, the impedance mismatching occurs because of the weaker coupling. Consequently, the absorption becomes slightly smaller. Further simulations are performed in Fig. 4(c) to verify the operation of MPA by varying the incident angle for TM polarization. Similarly to TE polarization, the single-peak absorption of 98.7% is obtained at 400 MHz for the normal incidence. For incident angle of 40°, the absorption remains at 92%, and the peak exhibits a slight blue-shift to 401 MHz. This blue-shift is quite consistent to the observed behavior in Ref. 38. These results confirm that the MPA maintains well the impedance-matching condition with the free space in a relatively wide range of the incident angle of EM wave up to 30° for both TE and TM polarization. Consequently, it can be concluded that the operation of designed MPA is not only established but promising for many practical applications.

In order to expand to practical application areas, we also propose a simple way to create dual-band perfect absorption based on self-asymmetric structure. According to the aforementioned analysis, only the fundamental magnetic resonance is excited by EM wave when the structure is symmetric. By increasing g_2, the symmetric structure is broken, leading to two different magnetic resonances are excited. Consequently, the dual-band perfect absorption is realized in the same region. Each resonance mode induces a separate absorption peak, which is controlled by the size of gaps (g_1,g_2). In this case, we optimized the dual-band MPA with thickness of 14.0 mm and g_1 is fixed to be 0.15 mm. Figure 5(a) presents the absorption spectra according to variation of g_2 for the normally incident plane wave. The single absorption peak is observed at 405 MHz when $g_1 = g_2 =$ 0.15 mm. When g_2 is changed to be 3.0 mm, two absorption peaks at 492 and 571 MHz are clearly observed due to the high asymmetry of structure. This yields absorption of 99.97% and 99.60% at lower and higher resonance frequencies, respectively. Both absorption peaks are the result of

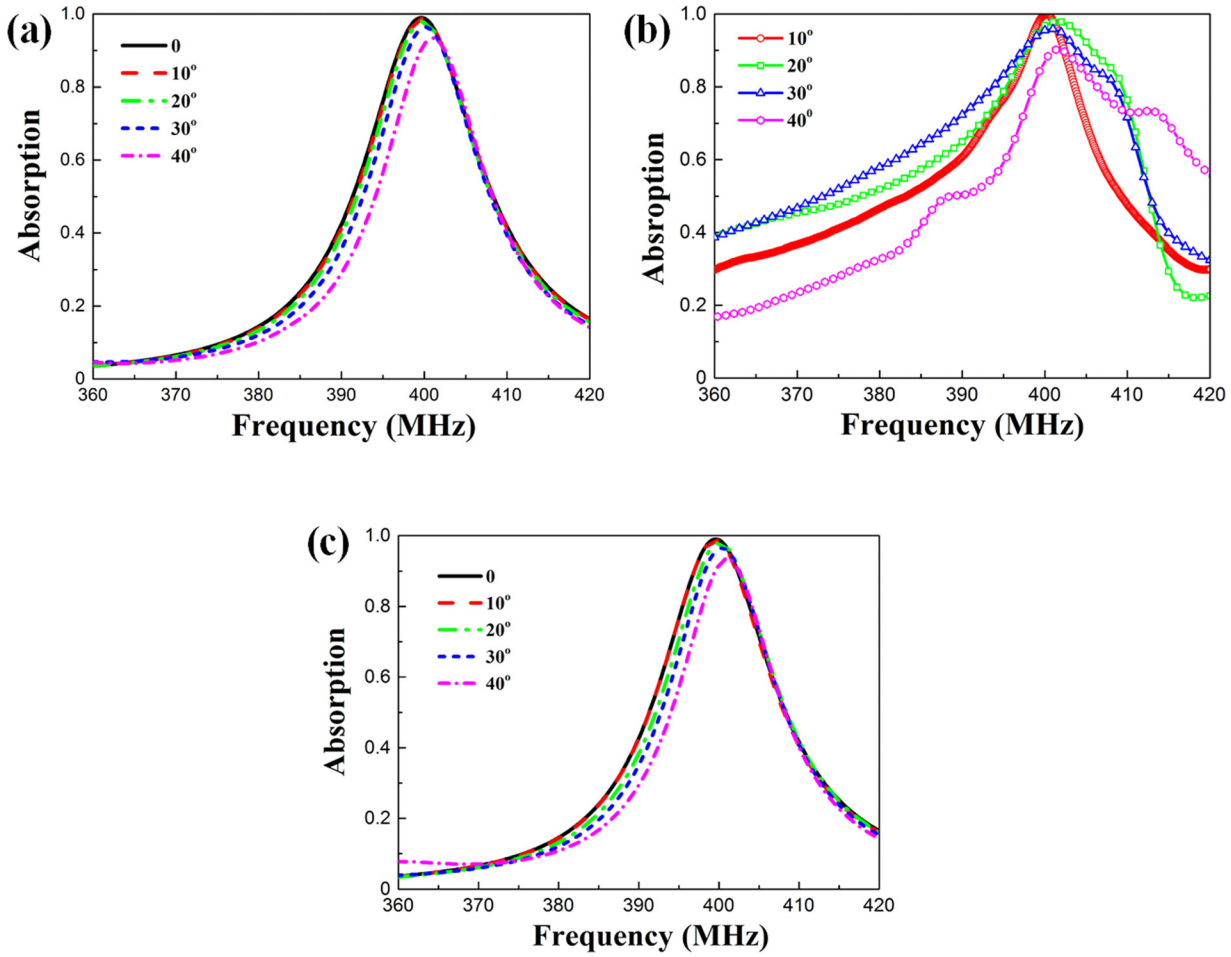

FIG. 4. (a) Simulated and (b) measured absorption spectra of single-peak MPA according to the incident angle of EM wave for TE polarization. (c) The same simulated absorption spectra for TM polarization.

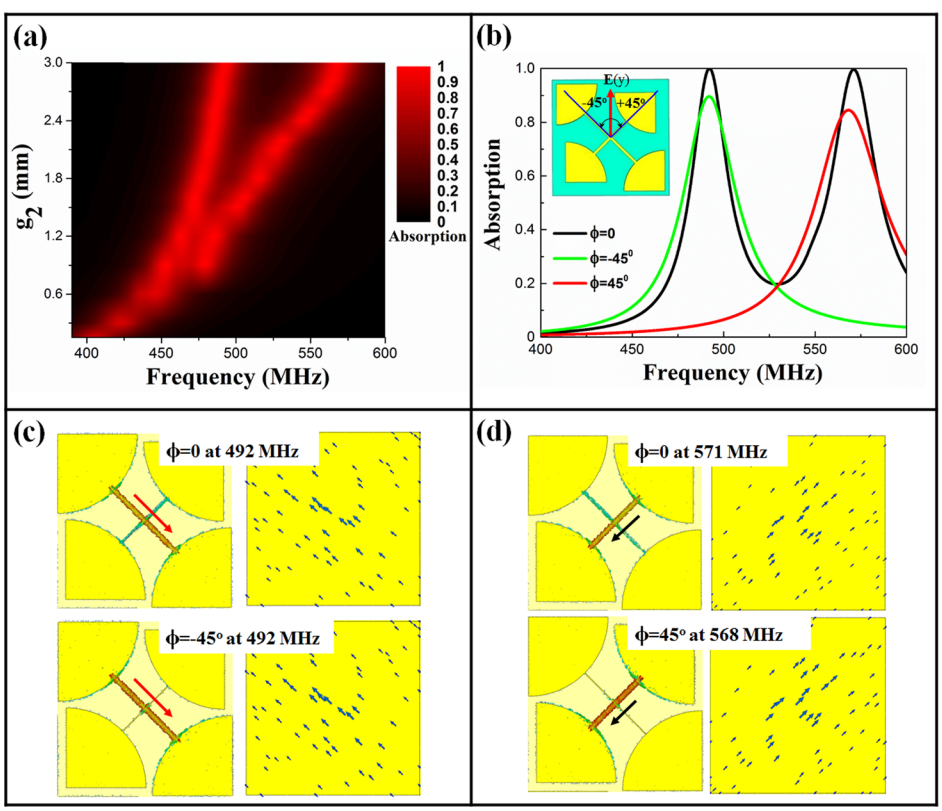

FIG. 5. (a) Dependence of the absorption on the gap (g_2) of proposed dual-band MPA. (b) Simulated absorption spectra according to the polarization angle (ϕ) of EM wave. The inset is the schematic view of varying polarization angle ϕ. Induced surface currents on the front and the back metallic layers at two absorption peaks for (c) $\phi = -45^\circ$ and (d) $\phi = 45^\circ$. Red and black arrows are designated for the current flows on the surface of front metallic layer at low and high absorption frequencies, respectively.

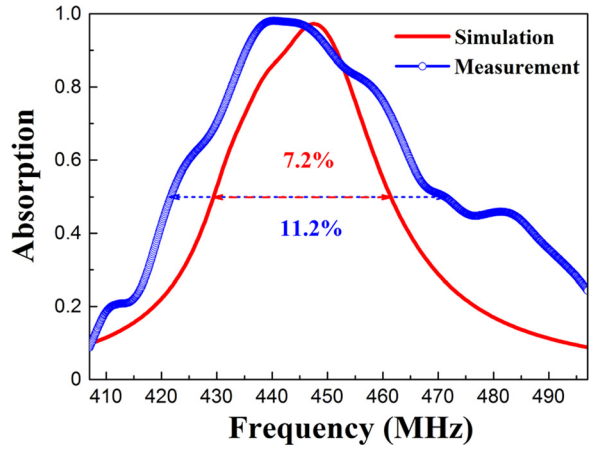

FIG. 6. Simulated and experimental absorption spectra of enhanced-bandwidth MPA with $g_2 = 0.6$ mm at incident angle of 10°. Red and blue dashed arrows are marked for the FWHM values of simulated and measured absorption spectra, respectively.

magnetic resonance, which is justified with anti-parallel surface currents on the front and the back metallic layers in Figs. 5(c) and 5(d). Obviously, the explicit separation into two absorption peaks is obtained if the self-asymmetry of structure is large.

To gain overall insight of the underlying mechanism of dual-band MPA, the dependence of absorption on the polarization of EM wave is investigated in Fig. 5(b). We set the polarization angle (ϕ) of EM wave to be 0, −45°, and 45°. For $\phi = -45°$ and 45°, it is clearly seen that the dual-band MPA is replaced by single peak at 492 and 568 MHz, respectively, which are close to the low and the high frequencies of dual-band absorption at $\phi = 0$. For more details, in Figs. 5(c) and 5(d), we compare the distributions of surface currents at two absorption frequencies for different ϕ. The surface current for $\phi = -45°$ (45°) is similar to that at low (high) absorption frequency for $\phi = 0$. Therefore, it can be concluded that the dual-band MPA is the combination of two modes, which are induced by the long and the short diagonal elements of structure [see Figs. 5(c) and 5(d)]. It should also be noted that the operation of dual-band MPA structure is sensitive to the polarization angle of EM wave. For that reason, the self-asymmetric feature can be useful for single/dual-band absorption switching by controlling the EM polarization.

Finally, the geometrical parameter g_2 is finely manipulated for two absorption peaks to be partly overlapped. Consequently, the FWHM of absorption spectrum is enhanced in the same range. In this case, we select the value of gap $g_2 = 0.6$ mm (g_1 is fixed to be 0.15 mm), which ensures that two absorption peaks are close enough. To explain this in detail, the simulated and the experimental absorption spectra of the suggested MPA are demonstrated

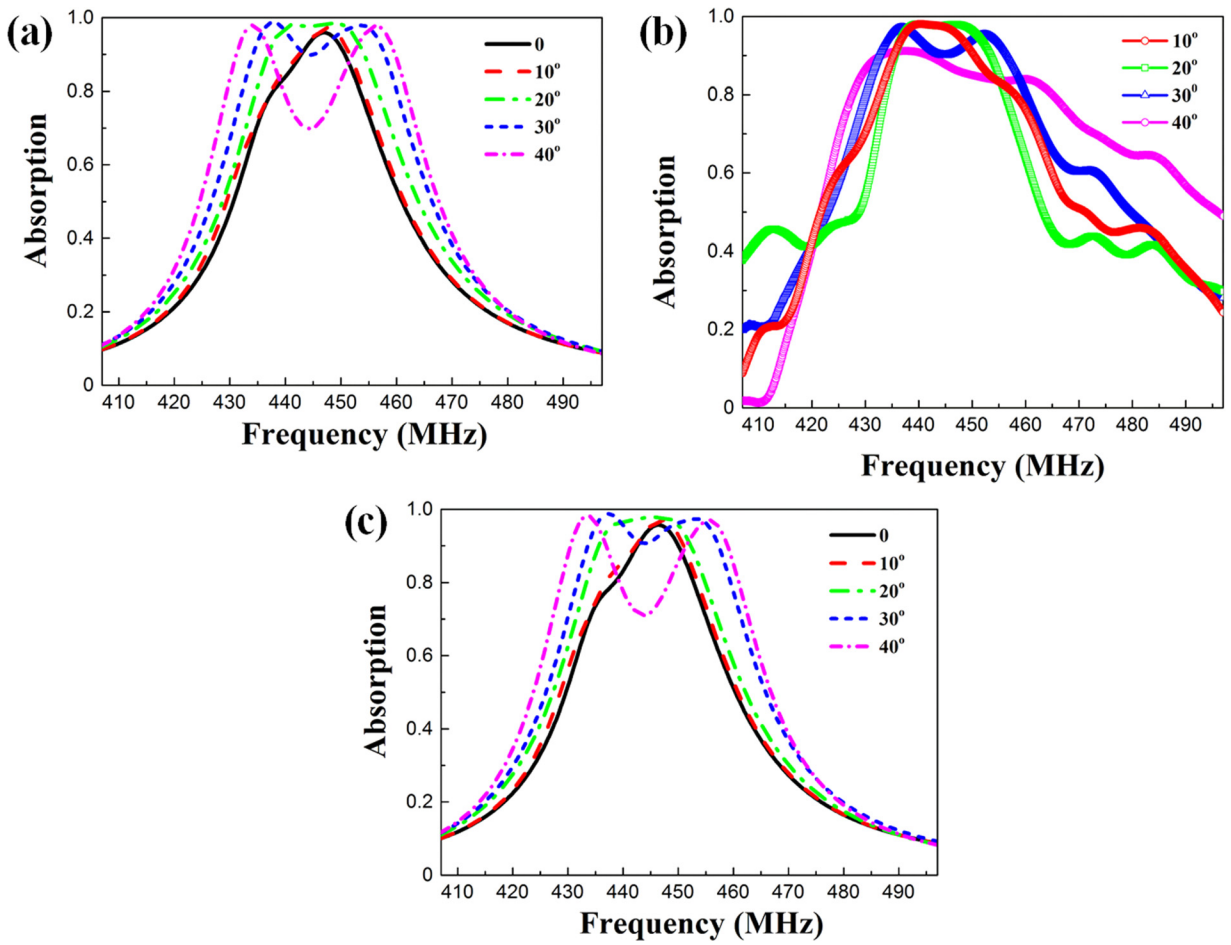

FIG. 7. (a) Simulated and (b) measured absorption spectra of enhanced-bandwidth MPA according to the incident angle of EM wave for TE polarization. (c) The same simulated absorption spectra for TM polarization.

in Fig. 6. In Fig. 2(a), the simulated and the measured FWHM values of single-peak MPA are only 4.0% and 6.3%, respectively. Meanwhile, by combining two resonances, the simulated and the measured values reach 7.2% and 11.2%, respectively. Therefore, the FWHM is nearly twice larger with respect to the case of single-peak MPA in both simulated and measured spectra.

Figures 7(a) and 7(b) present the evolution of simulated and measured absorption spectra according to the incident angle θ for TE polarization. It is clearly seen that the measured absorption spectra are in good agreement with the simulated ones. In Fig. 7(a), by increasing the incident angle from 10° to 30°, the absorption bandwidth continues to be extended from 10 to 24 MHz at absorption of 90%. The similar trend is observed in the experimental data in Fig. 7(b). The measured absorption bandwidth at absorption exceeding 90% is obtained between 433 and 457 MHz at $\theta = 30°$. For incident angle of 40°, the absorption peaks are evidently separated and the absorption remains less than 90%. The similar behavior has been observed for oblique illumination.[39] Furthermore, the operation of enhanced-bandwidth MPA by changing the incident angle for TM polarization is also evaluated in detail, as in Fig. 7(c). By comparing Figs. 7(a) and 7(c), the calculated FWHM and the tendency of absorption spectrum with respect to the incident angle for TM polarization turn out to be similar to those of TE polarization. On the other hand, the operational absorption bandwidth of MPA also keeps widening (from 10 up to 24 MHz at absorption of 90%) by changing the incident angle from 10° to 30° in TM polarizations. This finding is emphasized as the feasible alternative for enhanced-bandwidth MPA.

IV. CONCLUSIONS

We have designed, fabricated, and demonstrated single-peak MPA with thin thickness and small lattice constant. Due to the special design, absorption occurs at very low frequency. Both simulation and measurement confirm perfect absorption at 400 MHz, and the absorption is nearly unchanged in a relatively wide range (up to 30°) of the incident angle of EM wave for TE and TM polarization. The mechanism of absorption is also clarified through the surface-current and the magnetic-energy distributions, which is due to the magnetic resonance. The roles of structural components in MPA design to obtain low-frequency absorption are also explained in detail by both calculation and simulation. Furthermore, by flexibly controlling the geometry of MPA structure, we obtained the dual-band perfect absorption in the same region. The FWHM of single-peak MPA can be enhanced to be nearly twice. Especially, the extension of absorption bandwidth (for absorption of 90%) is well maintained at incident angle up to $\theta = 30°$ for both TE and TM polarization. Our work is expected to contribute to the development of future devices in the radio range.

ACKNOWLEDGMENTS

This work was supported by the ICT R&D Program of MSIP/IITP, Korea (KCA-2013-005-038-001).

[1]D. R. Smith, W. J. Padilla, D. C. Vier, S. C. Nemat-Nasser, and S. Schultz, Phys. Rev. Lett. **84**, 4184 (2000).
[2]D. Cheng, H. Chen, N. Zhang, J. Xie, and L. Deng, J. Opt. Soc. Am. B **30**, 224 (2013).
[3]V. T. T. Thuy, N. T. Tung, J. W. Park, V. D. Lam, Y. P. Lee, and J. Y. Rhee, J. Opt. **12**, 115102 (2010).
[4]M. S. Jang and H. Atwater, Phys. Rev. Lett. **107**, 207401 (2011).
[5]S. H. Mousavi, A. B. Khanikaev, J. Allen, M. Allen, and G. Shvets, Phys. Rev. Lett. **112**, 117402 (2014).
[6]N. Fang, H. Lee, C. Sun, and X. Zhang, Science **308**, 534 (2005).
[7]C. P. Scarborough, Z. H. Jiang, D. H. Werner, C. Rivero-Baleine, and C. Drake, Appl. Phys. Lett. **101**, 014101 (2012).
[8]D. Schurig, J. J. Mock, B. J. Justice, S. A. Cummer, J. B. Pendry, A. F. Starr, and D. R. Smith, Science **314**, 977 (2006).
[9]G. Pawlik, K. Tarnowski, W. Walasik, A. C. Mitus, and I. C. Khoo, Opt. Lett. **37**, 1847 (2012).
[10]M. C. K. Wiltshire, J. B. Pendry, I. R. Young, D. J. Larkman, D. J. Gilderdale, and J. V. Hajnal, Science **291**, 849 (2001).
[11]V. D. Lam, J. B. Kim, S. J. Lee, and Y. P. Lee, J. Appl. Phys. **103**, 033107 (2008).
[12]S. T. Bui, V. D. Nguyen, X. K. Bui, T. T. Nguyen, P. Lievens, Y. P. Lee, and D. L. Vu, J. Opt. **15**, 075101 (2013).
[13]C. Rockstuhl, T. Zentgraf, H. Guo, N. Liu, C. Etrich, I. Loa, K. Syassen, J. Kuhl, F. Lederer, and H. Giessen, Appl. Phys. B **84**, 219 (2006).
[14]J. Yao, Z. Liu, Y. Liu, Y. Wang, C. Sun, G. Bartal1, A. M. Stacy, and X. Zhang, Science **321**, 930 (2008).
[15]N. I. Landy, S. Sajuyigbe, J. J. Mock, D. R. Smith, and W. J. Padilla, Phys. Rev. Lett. **100**, 207402 (2008).
[16]X. Liu, T. Starr, A. F. Starr, and W. J. Padilla, Phys. Rev. Lett. **104**, 207403 (2010).
[17]X. Liu, T. Tyler, T. Starr, A. F. Starr, N. M. Jokerst, and W. J. Padilla, Phys. Rev. Lett. **107**, 045901 (2011).
[18]J. Hao, L. Zhou, and M. Qiu, Phys. Rev. B **83**, 165107 (2011).
[19]N. Liu, M. Mesch, T. Weiss, M. Hentschel, and H. Giessen, Nano Lett. **10**, 2342 (2010).
[20]J. Rosenberg, R. V. Shenoi, T. E. Vandervelde, S. Krishna, and O. Painter, Appl. Phys. Lett. **95**, 161101 (2009).
[21]T. Koschny, M. Kafesaki, E. N. Economou, and C. M. Soukoulis, Phys. Rev. Lett. **93**, 107402 (2004).
[22]M. Pu, C. Hu, M. Wang, C. Huang, Z. Zhao, C. Wang, Q. Feng, and X. Luo, Opt. Express **19**, 17413 (2011).
[23]H. Wakatsuchi, S. Greedy, C. Christopoulos, and J. Paul, Opt. Express **18**, 22187 (2010).
[24]P. V. Tuong, J. W. Park, J. Y. Rhee, K. W. Kim, W. H. Jang, H. Cheong, and Y. P. Lee, Appl. Phys. Lett. **102**, 081122 (2013).
[25]Y. J. Yoo, H. Y. Zheng, Y. J. Kim, J. Y. Rhee, J.-H. Kang, K. W. Kim, H. Cheong, Y. H. Kim, and Y. P. Lee, Appl. Phys. Lett. **105**, 041902 (2014).
[26]L. Huang, D. R. Chowdhury, S. Ramani, M. T. Reiten, S.-N. Luo, A. K. Azad, A. J. Taylor, and H.-T. Chen, Appl. Phys. Lett. **101**, 101102 (2012).
[27]P. Pitchappa, C. P. Ho, P. Kropelnicki, N. Singh, D.-L. Kwong, and C. Lee, Appl. Phys. Lett. **104**, 201114 (2014).
[28]D. S. Wilbert, M. P. Hokmabadi, P. Kung, and S. M. Kim, IEEE Trans. Terahertz Sci. Technol. **3**, 846 (2013).
[29]Y. Okano, S. Ogino, and K. Ishikawa, IEEE Trans. Microwave Theory Tech. **60**, 2456 (2012).
[30]S. Yagitani, K. Katsuda, M. Nojima, Y. Yoshimura, and H. Sugiura, IEICE Trans. Commun. **E94-B**, 2306 (2011).
[31]F. Costa, S. Genovesi, and A. Monorchio, IEEE Trans. Microwave Theory Tech. **61**, 146 (2013).
[32]F. Costa, S. Genovesi, A. Monorchio, and G. Manara, IEEE Antennas Wireless Propag. Lett. **8**, 1341 (2009).
[33]See http://www.cst.com for CST of America, Inc., 492 Old Connecticut Path, Suite 505 Framingham, MA 01701, USA.
[34]Y. J. Yoo, Y. J. Kim, P. V. Tuong, J. Y. Rhee, K. W. Kim, W. H. Jang, Y. H. Kim, H. Cheong, and Y. P. Lee, Opt. Express **21**, 32484 (2013).
[35]J. Zhou, E. N. Economou, T. Koschny, and C. M. Soukoulis, Opt. Lett. **31**, 3620 (2006).
[36]N. Zhang, P. Zhou, S. Wang, X. Weng, J. Xie, and L. Deng, Opt. Commun. **338**, 388 (2015).
[37]S. S. Mohan, Ph.D. thesis, Stanford University, 1999.
[38]J. Hao, J. Wang, X. Liu, W. J. Padilla, L. Zhou, and M. Qiu, Appl. Phys. Lett. **96**, 251104 (2010).
[39]K. B. Alici, A. B. Turhan, C. M. Soukoulis, and E. Ozbay, Opt. Express **19**, 14260 (2011).